chemosensors

MDPI

Article

A 4 × 4 Array of Complementary Split-Ring Resonators for Label-Free Dielectric Spectroscopy

Matko Martinic [1,*], Tomislav Markovic [1,2], Adrijan Baric [3] and Bart Nauwelaers [1]

[1] Division WaveCore, Department of Electrical Engineering (ESAT), KU Leuven, 3000 Leuven, Belgium; tomislav.markovic@imec.be (T.M.); bart.nauwelaers@kuleuven.be (B.N.)
[2] imec, 3001 Heverlee, Belgium
[3] Department of Electronics, Microelectronics, Computer and Intelligent Systems, Faculty of Electrical Engineering and Computing, University of Zagreb, 10000 Zagreb, Croatia; adrijan.baric@fer.hr
* Correspondence: matko.martinic@kuleuven.be

Abstract: In this study, complementary split-ring resonator (CSRR) metamaterial structures are proposed for label-free dielectric spectroscopy of liquids in microplates. This novel combination of an array of sensors and microplates is readily scalable and thus offers a great potential for non-invasive, rapid, and label-free dielectric spectroscopy of liquids in large microplate arrays. The proposed array of sensors on a printed circuit board consists of a microstrip line coupled to four CSRRs in cascade with resonant frequencies ranging from 7 to 10 GHz, spaced around 1 GHz. The microwells were manufactured and bonded to the CSRR using polydimethylsiloxane, whose resonant frequency is dependent on a complex relative permittivity of the liquid loaded in the microwell. The individual microstrip lines with CSRRs were interconnected to the measurement equipment using two electronically controllable microwave switches, which enables microwave measurements of the 4 × 4 CSRR array using only a two-port measurement system. The 4 × 4 microwell sensor arrays were calibrated and evaluated using water-ethanol mixtures with different ethanol concentrations. The proposed measurement setup offers comparable results to ones obtained using a dielectric probe, confirming the potential of the planar sensor array for large-scale microplate experiments.

Keywords: complementary split ring resonators; metamaterials; dielectric spectroscopy; complex permittivity; sensor array; resonator; microplate; microwell

Citation: Martinic, M.; Markovic, T.; Baric, A.; Nauwelaers, B. A 4 × 4 Array of Complementary Split-Ring Resonators for Label-Free Dielectric Spectroscopy. *Chemosensors* **2021**, *9*, 348. https://doi.org/10.3390/chemosensors9120348

Academic Editor: Patricia Khashayar

Received: 31 October 2021
Accepted: 7 December 2021
Published: 8 December 2021

1. Introduction

Microplates are nowadays used in many scientific areas as they enable time-efficient methods for simultaneously observing different chemical and biological events. A high number of small-volume wells, microwells, allows us to observe events in a small area without compromising high-throughput screening. Microplates are used in cell analysis [1–3], bacterial analysis [4], protein screening [5], enzyme screening [6], etc. Even though using microplate speeds up the processes by a great margin, it still takes time and expensive equipment to accurately monitor and quantify these events.

There are different methods to detect events in microplate wells. The traditional ones require the equipment called microplate reader, which relies on several different detecting methods that require some sort of chemical label. The three most often used methods are: (1) absorption measurements, measurement of transmitted light is used to calculate the concentration of a sample in a microwell, since light absorbed by the sample relates to its concentration [7]; (2) fluorescence measurements, the light emitted by fluorescent molecules that have been excited by a higher-level energy source is measured to calculate the concentration of a sample in a microwell [8]; (3) luminescence measurements, the light emitted from chemical reactions inside the well itself is captured to calculate the concentration [9].

Other methods do not require microplate readers but rather utilize different physical properties of the samples to detect and quantify reactions without any labels. With regards to the label-based sensing method, the label-free method is normally less time-consuming, less expensive, and more reliable as labels can alter cell properties [10]. In addition, the fluorescent labeling method used mostly for biochemical and molecular interactions cannot be used for the biophysical characterization of living cells [11]. In that manner, many different biosensors have been developed, such as optical biosensors employing photonic crystals [12], bioimpedance sensors [13], nanowire array sensors [14], and optical micro-ring resonator sensors [15].

Aside from previously described sensing approaches, microwave dielectric sensing is considered a great candidate for microplate sensing as it is a non-invasive, rapid, reliable, affordable, and precise measurement method. Dielectric spectroscopy was invented by physicist Peter Deby in 1912 as a technique suited for physics [16]. In the past century, it has become a well-established method for biological matter characterization [17] due to the strong dielectric contrast between various bio-species [18]. Variations in water content and physical parameters of a sample produce changes in the dielectric properties of the substance under test, raising the ability to analyze biomaterial without altering its biological state, which is essential for quantitative biology. The dielectric spectroscopy is performed by measuring the interaction between the biological sample and applied electrical field, and from that interaction, complex permittivity can be extracted [19]. By obtaining the complex permittivity of a sample, it is possible to calculate various parameters, such as cell size and concentration [20,21], cell interactions [22], antibody and antigen bindings [23], chemical reactions [24], etc. There are different ways to measure the complex permittivity of material, and the most traditional way is by using dielectric probes [25] or transmission lines loaded with a liquid of interest [22,26,27]. The more recent methods employ capacitive sensors [25,28–30] and or resonating structures [31–34]. In [29,33,35] the dielectric values of MUT obtained using label-free microwave sensing methods are comparable with values obtained using more established methods, demonstrating that microwave dielectric spectroscopy has the capabilities of determining a material's permittivity with high accuracy.

In this study, we utilize metamaterial-based resonating structures conceived around complementary split ring (CSRR) topology to exploit the influence of the complex permittivity of the loaded material on the resonant frequency of the CSRR. Metamaterials were first mentioned by Veselago in 1968 [36] as materials that exhibit negative permittivity and permeability not found in nature. All known materials have positive permittivity ε and permeability μ, except for ferrites that have negative μ at lower frequencies and metals that have negative ε near-visible frequencies [37]. When negative permeability and permittivity are obtained, wave vector k, magnetic H and electric E fields form a left-handed triplet resulting in an antiparallel group and phase velocity [38]. In addition, inversed Snell law, inversed Doppler effect and backward Cherenkov radiation are achievable.

One of the first and most researched two-dimensional metamaterial cells is a split ring resonator (SRR), shown in Figure 1a, and it has been so far used as a dispersionless filter [39], and as a sensor in microfluidics [40] and bio-sensing application [41], among many others. When coupled with a magnetic field perpendicular to its surface, the SRR exhibits negative permeability at a frequency above the self-resonant frequency. The SRR exhibits an electrical field between rings that is parallel to its surface resulting in a small penetration depth and sensitivity [38]. In addition to that, the distance between the two rings is too small to accommodate a microwell. This problem can be mitigated using a CSRR topology.

The CSRR metamaterial cell, shown in Figure 1b, is often used as a dielectric sensor [40,42–46]. It is a planar resonator, a dual counterpart of the SRR, with a subwavelength footprint and a high-quality factor with the electric field perpendicular to a circular patch in the middle, and with an already developed circuit model, which makes it a great candidate for microplate dielectric sensing compared with other metamaterials. When excited by the electric field perpendicular to its surface [38], the CSRR behavior

can be modeled with an electrical circuit, as shown in Figure 1c. *Lt* is the inductance of a microstrip line, *C* is a capacitance between the CSRR cell and a microstrip line, *Lc* is the inductance of the CSRR, and *εrCc* is the capacitance between the CSRR ring and the ground plane. The derived equation for a resonant frequency on which the LC network forms a short circuit that manifests as a total reflection is written in (1). Placing a material under test (MUT) on top of the resonator will change relative permittivity *εr* of a capacitance *Cc* which in turn will change the resonant frequency. It is often coupled with a microstrip transmission line etched into the ground plane on the other side. In that way, a high electric field coupling is ensured. In addition to that, multiple CSRRs operating on different frequencies can be coupled onto the same transmission line, each maintaining high-quality factor and high sensitivity, with a reported frequency shift of around 250 MHz per arbitrary unit of relative permittivity [42].

$$f = \frac{1}{2\pi\sqrt{L_c(C + \varepsilon_r C_c)}} \quad (1)$$

In this study, a novel method for microplate well event monitoring is conceived around a CSRR array, the combination of resonating structures and microwell array has not been demonstrated so far, according to the author's best knowledge. In [28], the impedance spectroscopy was used for 96-well microplate sensing at low frequencies up to 110 kHz utilizing a multiplexer system for interconnection between sensors and impedance analyzer. A system for dielectric measurements of cell cultures was proposed in [29], and it increased the frequency range of impedance spectroscopy by employing an additional transmission line sensor. Nevertheless, it is not compatible with microwells. A quad-band CSRR setup for dielectric characterization of material was reported in [42] with the highest frequency of 5.8 GHz. In the reported design, the diameter of the inner patch is altered between sensors to achieve the desired resonant frequencies, and the sensing was performed by covering the whole CSRR cell with a MUT. In this study, the CSRRs sensors are proposed with the highest resonant frequency of 9.8 GHz utilizing only the electrical field perpendicular to the inner patch for microplate dielectric sensing while keeping the same inner radius dimension *R* across all CSRRs.

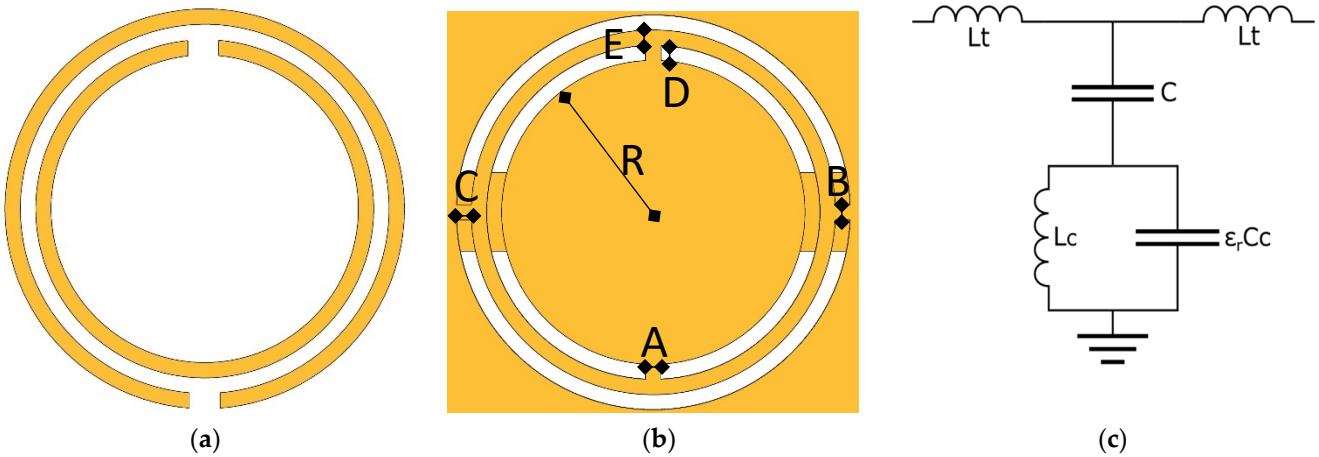

(**a**) (**b**) (**c**)

Figure 1. (**a**) A SRR metamaterial cell; (**b**) a CSRR cell etched below a microstrip line into the ground plane with important dimensions; (**c**) an equivalent circuit model of the CSRR cell.

In this work, we decided to excite four sensors at four distinct frequencies by using a single transmission line, which in turn allows us to characterize multiple events with a minimal number of microwave interconnects to the measurement equipment. Furthermore, the scaling of the proposed sensor array is easily achievable either by having more cascaded CSRR sensors on a single line or by having microwave switches to interconnect multiple lines with CSRRs. The proposed system was used for a rapid dielectric spectroscopy of

MUT, which was demonstrated using four water-ethanol mixtures with ethanol fractions of 20%, 40%, 60%, and 80%. The sensor arrays can measure the complex permittivity of the sample with comparable results to one obtained using a dielectric probe using significantly less volume in a small and compact design.

2. Materials and Methods

Dielectric characterization of the samples was performed using a Keysight slim form open-ended 200 mm coaxial probe (N1501A) (Keysight, 3110 Rotselaar, Belgium) connected to Keysight PNA (E8361A) (Keysight, 3110 Rotselaar, Belgium). The power level of PNA was set to −5 dBm with 30 Hz IF bandwidth and frequency ranging from 4 GHz to 7 GHz with 100 points in between, resulting in a total sweep time of 3 s. The temperature measurements were performed using the National Instruments USB-TC01 data acquisition device with thermocouple. The CSRRs were designed on a Rogers RO4350b printed circuit board (PCB) with a dielectric constant of 3.66, the thickness of 0.508 mm with 18 µm thick copper cladding, and gold coating of 5.1 µm. Microwell plates were fabricated using polydimethylsiloxane (PDMS) and a 3D printed mold using an in-house available standard 3D printer. The PDMS microplate wells were bonded to the PCB using a thin layer of PDMS. End launch subminiature version A (SMA) coaxial connectors were used to interconnect the CSRR sensor array to a Keysight M9735A vector network analyzer (VNA) and microwave switches. Two analog broadband non-reflective GaAs pHEMT microwave switches, HMC641ALC4 from Analog Devices (Analog Devices, Digi-Key, Enschede, The Netherlands), were used for fast switching between four sensor arrays. The switches do not only increase the reading speed, but they also decrease the equipment cost as only a two-port VNA is sufficient to evaluate multiple transmission lines with cascaded CSRR sensors. The VNA calibration was performed using a Keysight 85052D 3.5 mm calibration kit. The block diagram of a measurement system and calibration reference planes are shown in Figure 2. The first three CSRRs in each sensor array were used for dielectric sensing, while the last one was kept empty through measurements as a control sensor to demonstrate system stability. The measurements were carried out from 4 GHz to 9 GHz, using frequency spacing of 10 MHz (501 points), with the intermediate frequency (IF) bandwidth of 200 Hz and calibration correction turned on. The sweep time for the corresponding settings on used VNA was 2.52 s, which is relatively rapid given that other techniques require a longer measurement time. Furthermore, it is possible to use four distinctive frequency bands and follow the resonant frequency only and thus furthermore reduce the sweep time into the sub-second period. A DC power source E3631A from Agilent Technologies (Keysight, 3110 Rotselaar, Belgium) was used with Arduino Nano microprocessor to bias and automatically control microwave switches.

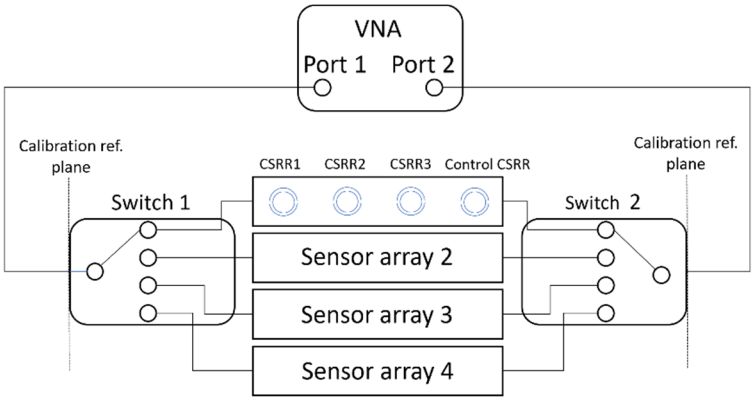

Figure 2. The block diagram of a measurement system with calibration reference planes.

2.1. CSRR Sensor Design

The CSRR was designed using the Advanced Design System (ADS) and Momentum software packages from Keysight. The four CSRR were etched into the ground plane of the same 50 Ω microstrip line with a center-to-center distance of 15 mm between two neighboring cells, see Figure 3a. We opted for circular sensors in this work as it has been shown [41] that they offer better sensitivity than rectangular sensors. In addition to that, the circular sensors have better compatibility with cylindric microwell plates. All CSRR cells were designed with the same middle circle patch radius *R*. To obtain a high-frequency operation of the CSRR with a middle patch radius of 2 mm, four splits were used. They bring an additional capacitance in series into the resonator, which lowers the total capacitance and consequently increases the resonant frequency of the CSRR. Altering the ring width *E*, splits widths *A* and *B*, and gaps *D* and *C*, shown in Figure 1b, four CSRRs with resonant frequencies of 6.9 GHz, 7.9 GHz, 8.9 GHz, and 9.8 GHz were designed. The designed sensors are shown in Figure 3a, while the final design dimensions are listed in Table 1.

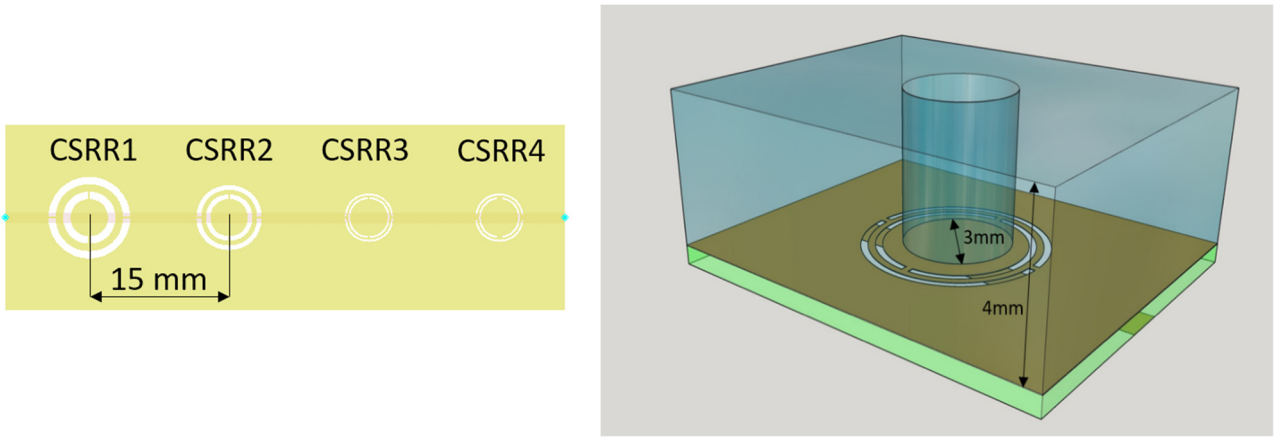

(**a**) (**b**)

Figure 3. (**a**) A microstrip line with four CSRRs etched into the ground plane; (**b**) a PDMS microwell on top of the CSRR.

Table 1. CSRRs resonant frequencies and dimensions.

	CSRR1	CSRR2	CSRR3	CSRR4
Resonant frequency [GHz]	6.9	7.9	8.9	9.8
R [mm]	2	2	2	2
A and B [mm]	0.2	0.2	0.2	0.6
C and D [mm]	0.8	0.5	0.2	0.2
E [mm]	0.8	0.5	0.2	0.2

2.2. Microwell Design

The microwells were manufactured using PDMS due to its versatility and extensive use as a microfluidic channel medium. A mold was manufactured using an in-house available 3D printer. The microwell is shown in Figure 3b with its dimensions, the base diameter is 3 mm, while the height is 4 mm, which translates into a volume of around 28 µL. The base diameter of the microwell is smaller than the diameter of the CSRR so that only the electric field sourced by the middle patch interacts with the MUT. We opted for such a design choice to ensure the high penetration depth of a sensor as electric field distribution in the middle is perpendicular to its surface. Finally, all microwells had the same overall CSRRs.

3. Results

3.1. Dielectric Probe Measurements of the Samples

In order to determine the relative complex permittivity of the samples, measurements were conducted using the dielectric probe with the measurement setup shown in Figure 4a. In total 8 samples of water-ethanol mixture with ethanol concentration ranging from 10% up to 80% in steps of 10% were prepared by mixing 96% medical ethanol with distilled water. The mixing was performed in a glass container, with each sample having the same volume of 15 mL. Dielectric probe measurement was performed twice for each sample, before and after loading sensors, to determine the change in permittivity of the sample as the portion of the ethanol evaporated during the time it took to load sensors. The change in permittivity of a sample with 70% ethanol concentration can be observed in Figure 4b. To ensure permittivity change is only due to ethanol evaporation, the temperature of the samples was recorded before each probe measurement. The temperature of all samples was around 20 °C with a maximum difference of 0.4 °C recorded between the two probe measurements indicating the temperature stability.

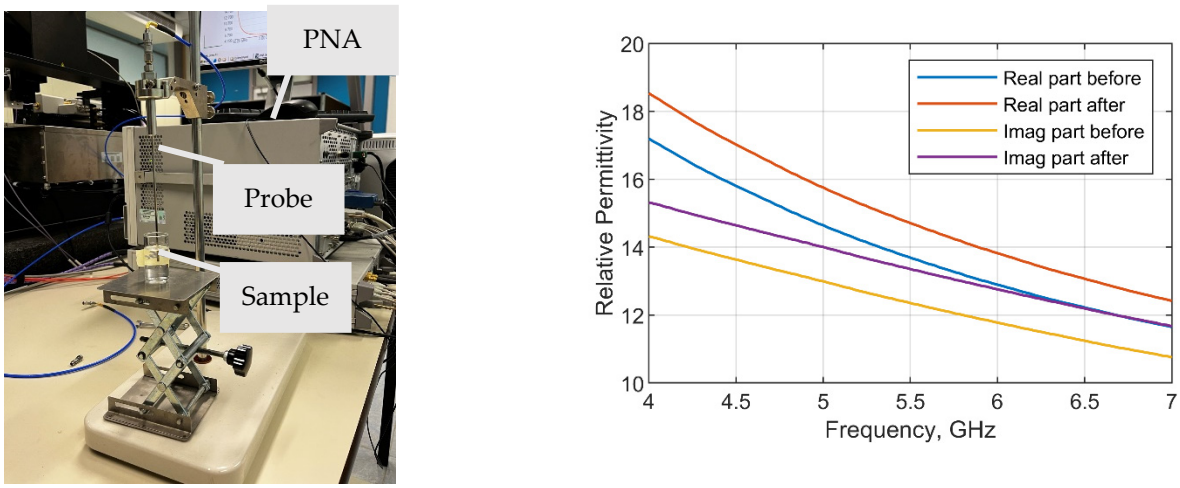

(**a**) (**b**)

Figure 4. (**a**) Probe measurement setup; (**b**) real and imaginary part of the relative permittivity of water-ethanol mixture with 70% ethanol fraction before and after loading microwells.

3.2. ADS Simulations and Measurements Loaded CSRRs with Air

As stated previously, the CSRR in this work was used as a sensor. In other words, once the middle patch of the CSRR is loaded with a MUT, the resonant frequency of the resonator changes. Initially, CSRRs were designed without the PDMS microwell, and the corresponding simulation results of individual resonators are shown in Figure 5a. As can be noticed in Figure 5a, two types of simulations were carried out. Based on these results, we can conclude that the faster method of moments (MoMs) simulations yield comparable results to the slower finite element method (FEM) simulations. Afterward, four resonators were cascaded in the ascending order based on resonant frequencies. As it is our goal to create an array of transmission lines with CSRRs, multiple lines were manufactured and evaluated. The measured frequency responses of a transmission line with the sensor array, shown in Figure 5b, shows good agreement with simulation data in Figure 5a, given that connectors are positioned and mounted manually.

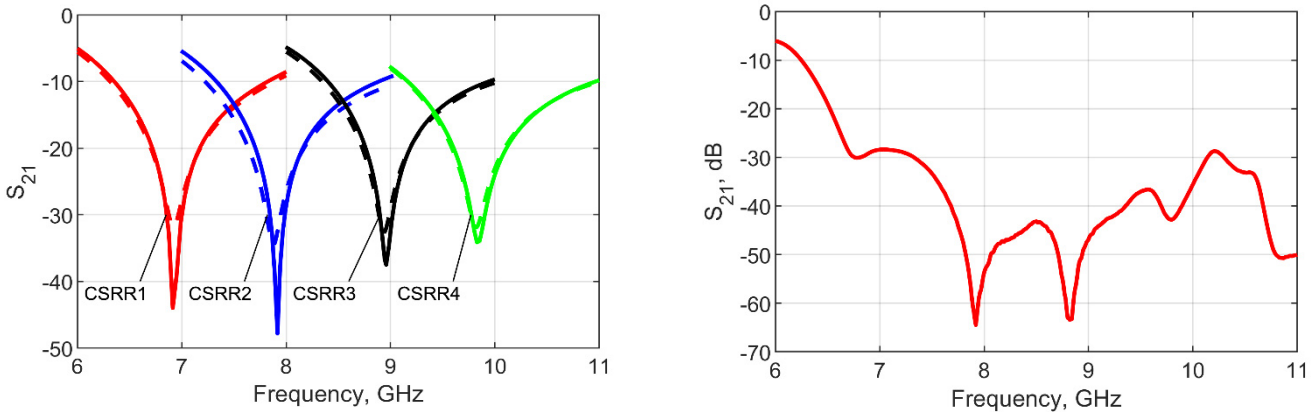

(**a**) (**b**)

Figure 5. (**a**) A frequency response of four individual CSRRs etched into the ground plane of a 50 Ω microstrip line, solid line represents MoM simulations and dashed line represents FEM simulations; (**b**) a measured frequency response of four CSRRs in cascade.

3.3. Measurements of Loaded and Interconnected CSRRs with PDMS Microwells

The PDMS loading influences the resonant frequency of the CSRR as it is in the gaps between a middle patch and ring, and ring and ground plane. In Figure 3b, it is shown that PDMS covers everything except the middle part of the CSRR patch where MUT is placed. Figure 6a shows the measured devices, and Figure 6b shows the measured transmission coefficients of all structures having the PDMS on top. Because PDMS has higher relative permittivity than the air of 2.8 and loss tangent of 0.016 at 5 GHz, the resonant frequencies of all devices are lower when compared with the case without PDMS, shown in Figure 5b. The first and second resonant frequencies can be observed around 5.5 GHz and 6.5 GHz, while the third and fourth resonant frequencies can be observed around 7.6 GHz and 8.2 GHz. Finally, the four lines with sensor arrays were interconnected using microwave switches, shown in Figure 6c, and the corresponding microwave measurements of transmission coefficients are presented in Figure 6d. As expected, there are additional losses existing in the transmission path due to the microwave switches and additional coaxial cables used for interconnection.

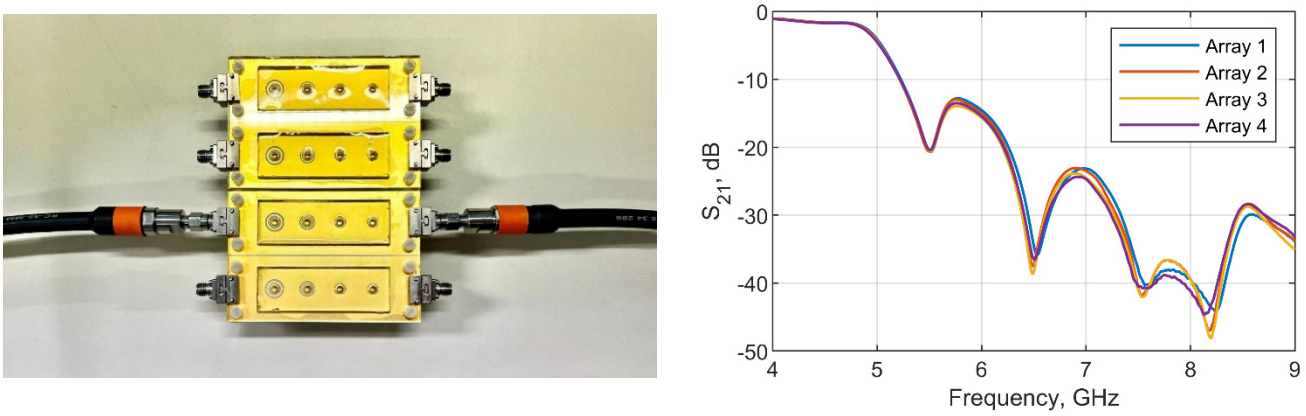

(**a**) (**b**)

Figure 6. *Cont.*

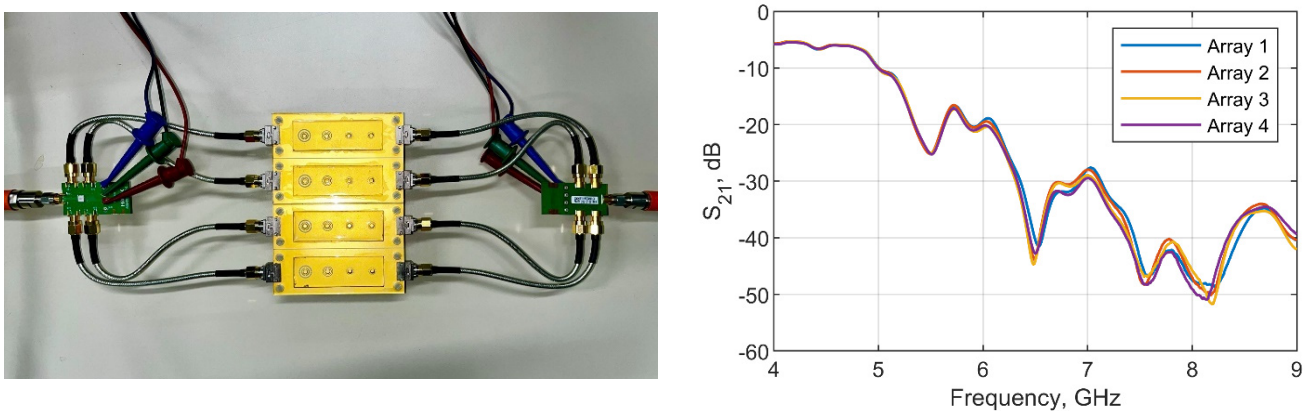

(**c**) (**d**)

Figure 6. (**a**) Sensor arrays 1 to 4 having empty PDMS microplate wells; (**b**) the transmission frequency response of structures having empty PDMS microplate wells; (**c**) interconnected sensor arrays 1 to 4 having PDMS microplate wells with microwave switches and coaxial cables; (**d**) the transmission frequency response of sensor arrays with PDMS and switches.

3.4. Dielectric Sensor Calibration and MUT Measurement Results

The microwave measurements in Sections 3.2 and 3.3 were carried out to verify the design and to investigate the influence of microwave switches on the total performance of the sensor array. In this section, the mathematical model is derived according to [40], where the complex permittivity of a sample can be determined by measuring the change in resonant frequency and peak attenuation. The simple linear model written in (2) is used where $\Delta f = f_{MUT} - f_{ref}$, $\Delta|S_{21}| = |S_{21,MUT}| - \left|S_{21,ref}\right|$, $\Delta\varepsilon' = \varepsilon'^{MUT} - \varepsilon'^{ref}$ and $\Delta\varepsilon'' = \varepsilon''^{MUT} - \varepsilon''^{ref}$, f indicating resonant frequency, S_{21} indicating peak attenuation, ε' and ε'' indicating the real and imaginary part of relative complex permittivity, respectively. Subscript MUT indicates values obtained when measuring material under test where subscript ref indicates reference sample–here water-ethanol mixture with an ethanol concentration of 50% is chosen as a reference sample.

$$\begin{bmatrix} \Delta f \\ \Delta|S_{21}| \end{bmatrix} = \begin{bmatrix} m_{11} & m_{12} \\ m_{21} & m_{22} \end{bmatrix} \begin{bmatrix} \Delta\varepsilon' \\ \Delta\varepsilon'' \end{bmatrix} \tag{2}$$

In order to obtain m-matrix coefficients, sensors CSRR1, 2, and 3 were loaded with four different samples with known relative complex permittivity obtained from probe measurements, while CSRR4 was kept empty as a reference throughout measurements to evaluate the drift of the measurement equipment. The transmission frequency response of each array is shown in Figure 7, with arrows indicating observed resonant frequencies. The least-square fitting method was used to determine coefficients as using four known samples makes the system of equations overdetermined. In total, 20 µL of each sample was loaded into each microwell using a pipette. After determining m-matrix coefficients, Equation (2) can be multiplied on the left side by inverse m-matrix resulting in Equation (3).

$$\begin{bmatrix} \Delta\varepsilon' \\ \Delta\varepsilon'' \end{bmatrix} = \begin{bmatrix} m_{11} & m_{12} \\ m_{21} & m_{22} \end{bmatrix}^{-1} \begin{bmatrix} \Delta f \\ \Delta|S_{21}| \end{bmatrix} \tag{3}$$

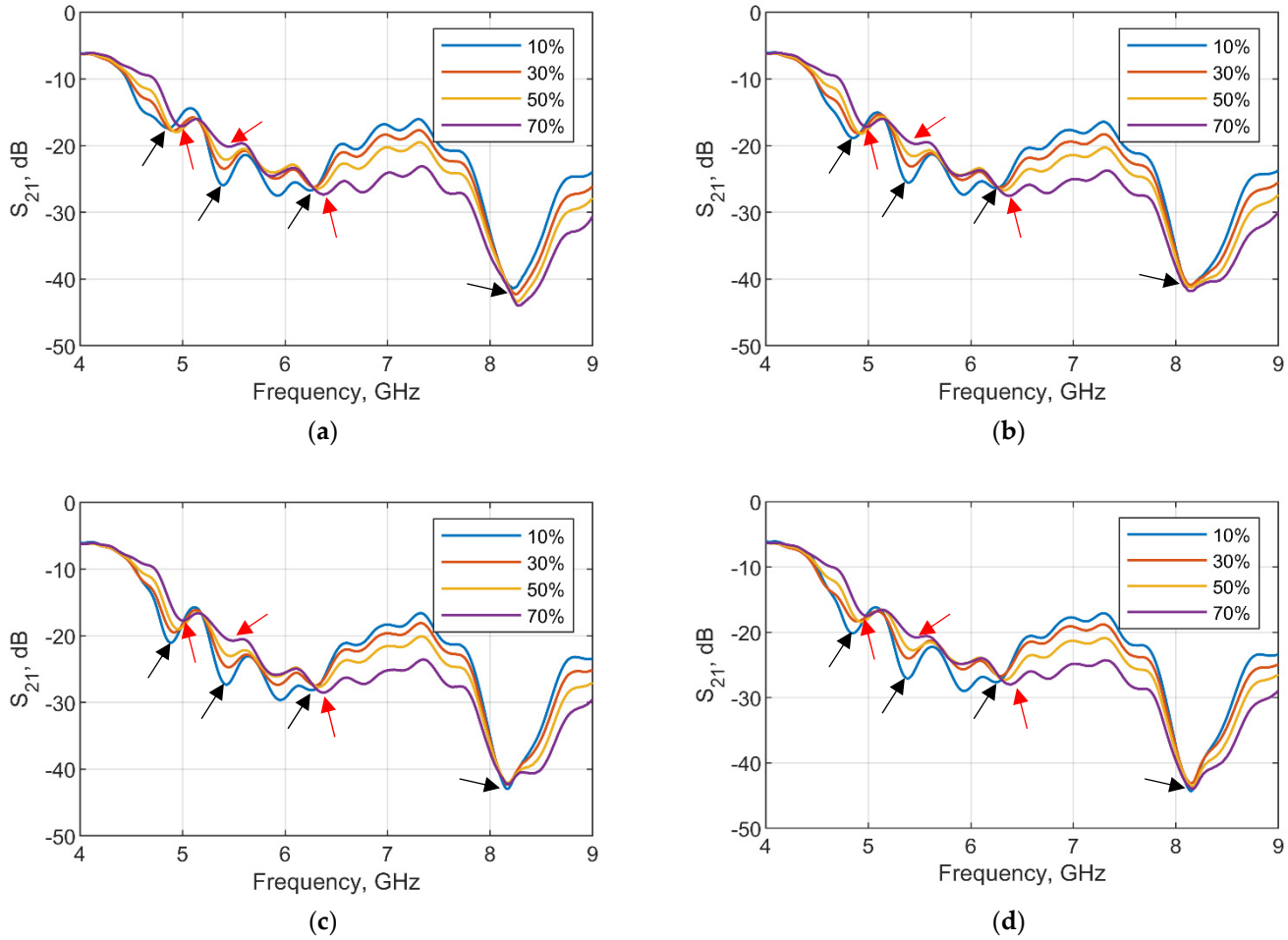

Figure 7. Transmission frequency response of the sensor array (**a**) 1, (**b**) 2, (**c**) 3, and (**d**) 4 filled with water-ethanol mixtures used for calibration with ethanol fraction of 10%, 30%, 50%, 70%.

According to Equation (3), by knowing the transmission frequency response of the sensor, it is possible to determine the complex permittivity of a MUT. To verify the mathematical model, the set of samples with an ethanol concentration of 20%, 40%, 60%, and 80% was used. The resonant frequency observed while measuring each sample was linearly increasing with ethanol percentage shown in Figure 8. On the other hand, the change in peak attenuation was not linear, shown in Figure 9. Finally, the calculated relative complex permittivity of the samples using CSRR1, 2, and 3 in array 1, compared with the one obtained using a dielectric probe, is shown in Figure 10.

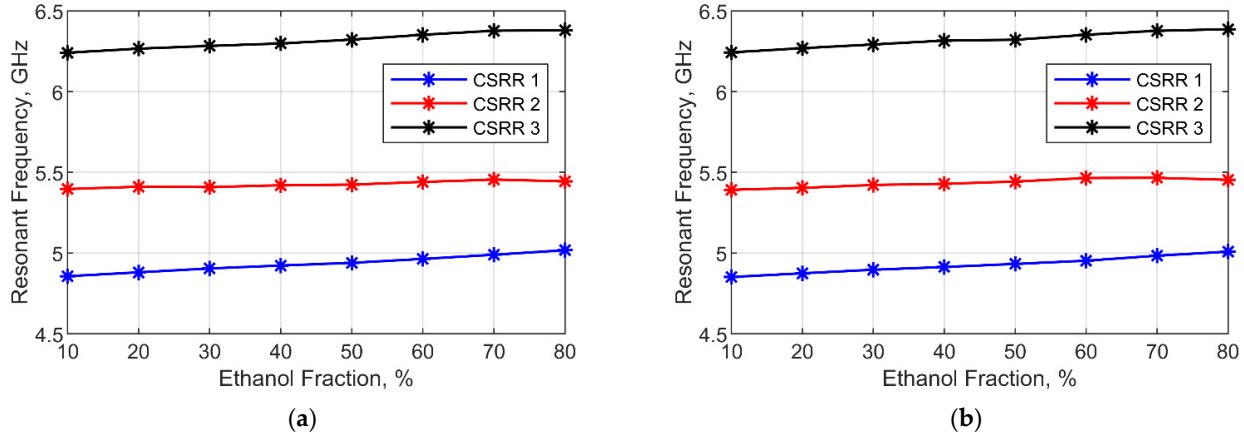

Figure 8. *Cont.*

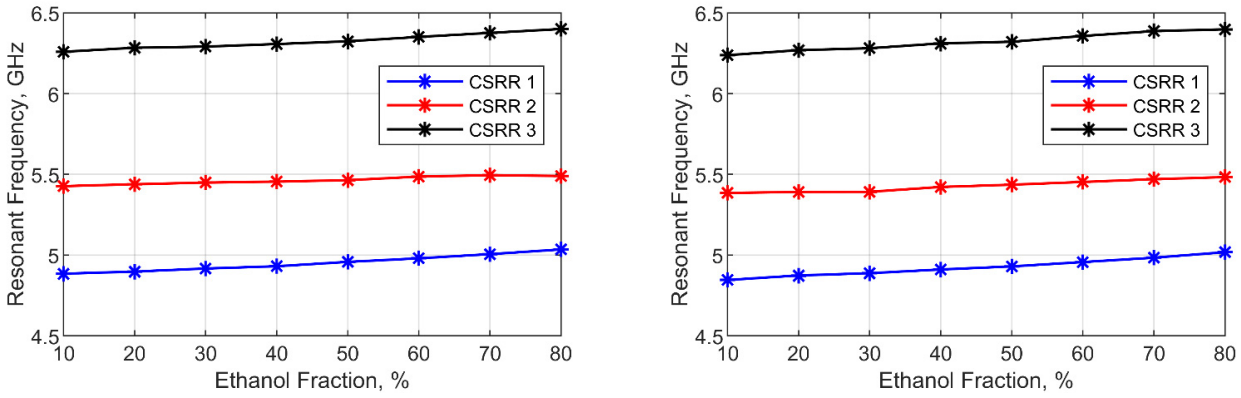

Figure 8. Observed resonant frequency shifts of the sensors in array (**a**) 1, (**b**) 2, (**c**) 3, and (**d**) 4 when filled with water-ethanol mixtures with different ethanol fraction.

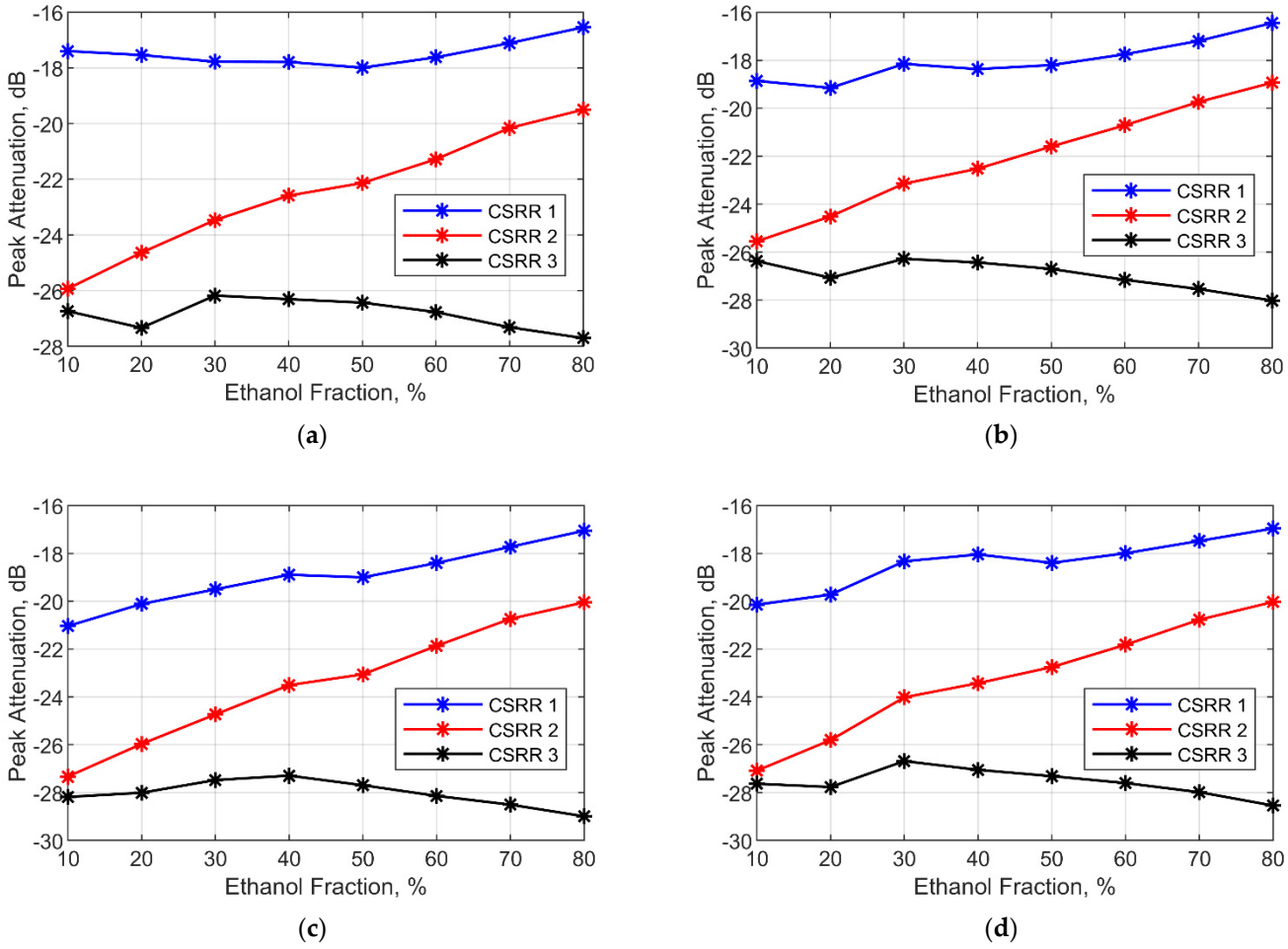

Figure 9. Observed attenuation peak values of the sensor array (**a**) 1, (**b**) 2, (**c**) 3, and (**d**) 4 when filled with water-ethanol mixtures with different ethanol fraction.

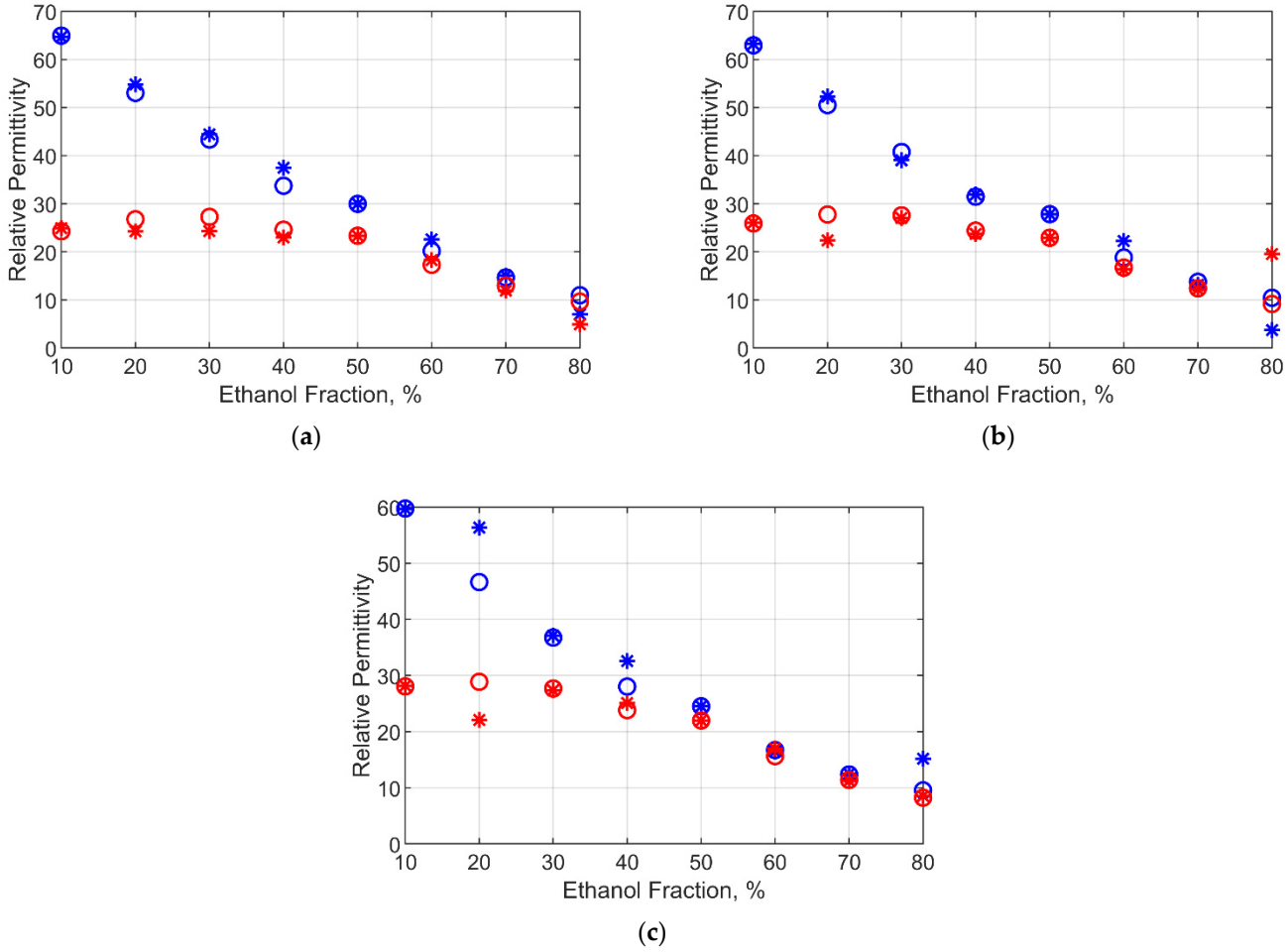

Figure 10. Relative permittivity of the samples obtained using sensors in array 1 (**a**) CSRR1, (**b**) CSRR2, (**c**) CSRR3 as stars, and values obtained using dielectric probe as circles, with blue indicating real part and red indicating imaginary part.

4. Discussion

During the dielectric characterization of samples using the dielectric probe, a substantial difference was observed in the complex permittivity of a sample before and after loading sensors. In Figure 4b, a maximum difference of 8% in a real part of relative permittivity between two measurements was measured; higher relative permittivity was observed after loading sensors indicating a higher concentration of water in the sample than before due to ethanol evaporation. To compensate for relative permittivity change in a sample, for arrays 1 and 4, the permittivity of the sample was assumed to be the same as probe measurements before and after loading microwells, respectively. For array 2, 1/3 of the difference between two probe measurements were added to permittivity measured before, and similarly, 2/3 were added for array 3.

The comparison of data in Figure 5a,b shows that there is a good match between designed and manufactured CSRRs with respect to the resonant frequency, which confirms the design approach and methodology. The transmission coefficient levels are lower when four CSRRs are connected in a cascade due to a change in the characteristic impedance of the transmission line on frequencies higher than CSRRs resonant frequency generating additional reflections and losses. Furthermore, the data comparison in Figure 6b,d shows the additional losses brought by switches in the measurement path. Nevertheless, those additional losses are taken into account by sensor calibration.

The microwells fabricated of PDMS were manually positioned and bonded to the PCB having sensor arrays. The microwells fabrication was performed with the same 3D printed mold to decrease variation between different sets of microwells as the diameter variation

and position of microwells can introduce additional uncertainties. This manual process brings additional variability between the frequency response of several sensor arrays, as can be observed in data in Figure 6b. Nevertheless, a more accurate fabrication process can mitigate the errors originating from the positioning and bonding of the microwells to the PCB. On the other hand, a more noticeable difference can be observed in Figure 6d between structures once additional cables and microwave switches were used. This difference can be mitigated in the future by integrating switches and sensor arrays onto the same PCB.

The measurement results of calibration samples in Figure 7 show five distinct local minimums for each sensor array with black and red arrows indicating observed local minimums for 10% and 70% ethanol concertation, respectively. The third local minimum did not experience a change in frequency when loaded with different samples, indicating it is due to additional reflection rather than the resonating frequency of CSRR3. The proposed system has distinctive resonant frequencies while sensing samples with different polarities and losses, suggesting the possibility of sensing a large variety of samples. Possible limitations can arise from sensing the samples with high losses, which will decrease the quality factor of resonators, making it more difficult to precisely determine the resonant frequency or even overlap with a frequency response of the neighboring sensor. Further research is required to quantify these system limitations. Furthermore, the resonant frequency of CSRR4 in array 1 does change for around 70 MHz during calibration, which can be attributed to additional reflection and losses from interconnections as well, while in other arrays, it stays the same indicating stability of the measurement setup.

The change in resonant frequency and peak attenuation for each sensor is shown in Figures 8 and 9. The resonant frequency observed while measuring each sample is linearly increasing with the ethanol percentage increase, which is expected as the real part of complex permittivity linearly decreases with an increase in ethanol concentration. On the other hand, the change in peak attenuation is nonlinear due to nonlinear change in the imaginary part of complex permittivity, shown in Figure 9. Finally, the derived complex permittivity values using the mathematical model from Section 3.4 were plotted against results obtained using the dielectric probe in Figure 10. The smallest deviation in real part was obtained by CSRR1, which was expected as it has a linear change in resonant frequency with change in ethanol concentration. On the other hand, peak attenuation change in CSRR3 follows the same function as a change in the imaginary part of the samples, resulting in the highest accuracy when determining the imaginary part of permittivity. This observation is in agreement with results in [40], the change in resonant frequency is due to a change in real part, and the change in attenuation level is due to change in dielectric losses introduced by MUT. The discrepancy in the imaginary part of complex permittivity in Figure 10c for 20% mixture in CSRR3 can be justified by deviation from the expected value in peak attenuation; similar values can be expected in other arrays as well due to a similar change in peak attenuation. Additional research is required to clarify these deviations. Furthermore, the calibration was performed for every sensor, nevertheless, similar results were obtained for all sensor arrays while using the calculated calibration coefficients of array 1, indicating similar behavior of sensors across all arrays and the future possibility to calibrate only one array, which in turn reduces calibration time significantly.

In conclusion, our proposed approach for monitoring events in microplates based on an array of cascaded CSRR sensors multiplexed over several transmission lines shows great potential for laboratory life science applications. It allows rapid, label-free, automated, and non-invasive sensing of relative complex permittivity in biological materials and liquids while offering at the same time scalability and affordability for numerous applications.

Author Contributions: Conceptualization, T.M. and M.M.; methodology, M.M. and T.M.; validation, T.M. and M.M.; formal analysis, M.M. and T.M.; investigation, M.M. and T.M.; resources, T.M., A.B. and B.N.; writing—original draft preparation, M.M. and T.M.; writing—review and editing, T.M., A.B. and B.N.; visualization, M.M. and T.M.; supervision, A.B. and B.N.; funding acquisition, T.M. and B.N. All authors have read and agreed to the published version of the manuscript.

Funding: This research was funded by the Research Foundation Flanders (FWO) Research Project under the grant number G0A1220N (MISTIQUE).

Institutional Review Board Statement: Not applicable.

Informed Consent Statement: Not applicable.

Conflicts of Interest: The authors declare no conflict of interest.

References

1. Lindström, S.; Eriksson, M.; Vazin, T.; Sandberg, J.; Lundeberg, J.; Frisén, J.; Andersson-Svahn, H. High-Density Microwell Chip for Culture and Analysis of Stem Cells. *PLoS ONE* **2009**, *9*, e6997. [CrossRef] [PubMed]
2. Lindström, S.; Larsson, R.; Andersson-Svahn, H. Towards High-Throughput Single Cell/Clone Cultivation and Analysis. *Electrophoresis* **2008**, *6*, 1219–1227. [CrossRef]
3. Zhang, Q.; Zhang, J.; Shen, J.; Silva, A.; Dennis, D.A.; Barrow, C.J. A Simple 96-Well Microplate Method for Estimation of Total Polyphenol Content in Seaweeds. *J. Appl. Phycol.* **2006**, *18*, 445–450. [CrossRef]
4. Fowler, P.W.; Cruz, A.L.G.; Hoosdally, S.J.; Jarrett, L.; Borroni, E.; Chiacchiaretta, M.; Rathod, P.; Lehmann, S.; Molodtsov, N.; Walker, T.M.; et al. Automated Detection of Bacterial Growth on 96-Well Plates for High-Throughput Drug Susceptibility Testing of Mycobacterium Tuberculosis. *Microbiology* **2018**, *164*, 1522–1530. [CrossRef]
5. Pitt, A.M.; Lee, C. High Throughput Screening Protein Kinase Assays Optimized for Reaction, Binding, and Detection Totally Within a 96-Well Plate. *J. Biomol. Screen.* **1996**, *1*, 47–51. [CrossRef]
6. Arain, S.; John, G.T.; Krause, C.; Gerlach, J.; Wolfbeis, O.S.; Klimant, I. Characterization of Microtiterplates with Integrated Optical Sensors for Oxygen and pH, and Their Applications to Enzyme Activity Screening, Respirometry, and Toxicological Assays. *Sens. Actuat. B-Chem.* **2006**, *113*, 639–648. [CrossRef]
7. Marešová, L.; Sychrová, H. Applications of a Microplate Reader in Yeast Physiology Research. *Biotechniques* **2007**, *43*, 667–672. [CrossRef] [PubMed]
8. Wang, H.; Joseph, J.A. Quantifying Cellular Oxidative Stress by Dichlorofluorescein Assay Using Microplate Reader. *Free Radic. Biol. Med.* **1999**, *27*, 612–616. [CrossRef]
9. Yang, X.; Janatova, J.; Andrade, J.D. Homogeneous Enzyme Immunoassay Modified for Application to Luminescence-Based Biosensors. *Anal. Biochem.* **2005**, *336*, 102–107. [CrossRef] [PubMed]
10. Dalmay, C.; Pothier, A.; Cheray, M.; Lalloue, F.; Jauberteau, M.O.; Blondy, P. Label-free RF biosensors for human cell dielectric spectroscopy. *Int. J. Microw. Wirel. Technol.* **2009**, *6*, 497–504. [CrossRef]
11. Liu, A.Q.; Huang, H.J.; Chin, L.K.; Yu, Y.F.; Li, X.C. Label-free detection with micro optical fluidic systems (MOFS): A review. *Anal. Bioanal. Chem.* **2008**, *7*, 2443–2452. [CrossRef]
12. Cunningham, B.T.; Li, P.; Schulz, S.; Lin, B.; Baird, C.; Gerstenmaier, J.; Genick, C.; Wang, F.; Fine, E.; Laing, L. Label-free assays on the BIND system. *J. Biomol. Screen.* **2004**, *6*, 481–490. [CrossRef]
13. Ciambrone, G.J.; Liu, V.F.; Lin, D.C.; McGuinness, R.P.; Leung, G.K.; Pitchford, S. Cellular Dielectric Spectroscopy: A Powerful New Approach to Label-Free Cellular Analysis. *J. Biomol. Screen.* **2004**, *9*, 467–480. [CrossRef]
14. Gao, Z.; Agarwal, A.; Trigg, A.D.; Singh, N.; Fang, C.; Tung, C.H.; Fan, Y.; Buddharaju, K.D.; Kong, J. Silicon nanowire arrays for label-free detection of DNA. *Anal. Chem.* **2007**, *9*, 3291–3297. [CrossRef] [PubMed]
15. Washburn, A.L.; Gunn, L.C.; Bailey, R.C. Label-Free Quantitation of a Cancer Biomarker in Complex Media Using Silicon Photonic Microring Resonators. *Anal. Chem.* **2009**, *81*, 9499–9506. [CrossRef]
16. Woodward, W.H. Broadband Dielectric Spectroscopy—A Practical Guide. In *Broadband Dielectric Spectroscopy: A Modern Analytical Technique*; American Chemical Society: Washington, DC, USA, 2021; pp. 3–59.
17. Grenier, K.; Dubuc, D.; Chen, T.; Artis, F.; Chretiennot, T.; Poupot, M.; Fournie, J.J. Recent advances in microwave-based dielectric spectroscopy at the cellular level for cancer investigations. *IEEE Trans. Microw. Theory Tech.* **2013**, *5*, 2023–2030. [CrossRef]
18. Dubuc, D.; Mazouffre, O.; Llorens, C.; Taris, T.; Poupot, M.; Fournié, J.J.; Begueret, J.B.; Grenier, K. Microwave-based biosensor for on-chip biological cell analysis. *Analog Integr. Circuits Signal Process.* **2013**, *2*, 135–142. [CrossRef]
19. Artis, F.; Chen, T.; Chretiennot, T.; Fournie, J.J.; Poupot, M.; Dubuc, D.; Grenier, K. Microwaving biological cells: Intracellular analysis with microwave dielectric spectroscopy. *IEEE Microw. Mag.* **2015**, *4*, 87–96. [CrossRef]
20. Morgan, H.; Sun, T.; Holmes, D.; Gawad, S.; Green, N.G. Single cell dielectric spectroscopy. *J. Phys. D Appl. Phys.* **2006**, *1*, 61. [CrossRef]
21. Bao, X.; Ocket, I.; Crupi, G.; Schreurs, D.; Bao, J.; Kil, D.; Puers, B.; Nauwelaers, B. A planar one port microwave microfluidic sensor for microliter liquids characterization. *IEEE J. Electromagn. RF Microw. Med. Biol.* **2018**, *1*, 10–17. [CrossRef]
22. Chen, Q.; McMurdie, J.; Roitman, D.; Knoesen, A. Microwave transmission line dielectric probe to detect biomolecular surface interactions. In Proceedings of the 26th Annual International Conference of the IEEE Engineering in Medicine and Biology Society, San Francisco, CA, USA, 1 September 2004.
23. Go, R.; Bashir, R.; Sarikaya, A.; Ladisch, M.R.; Sturgis, J.; Robinson, J.P.; Geng, T.; Bhunia, A.K.; Apple, H.L.; Wereley, S. Microfluidic biochip for impedance spectroscopy of biological species. *Biomed. Microdevices* **2001**, *3*, 201–209.
24. Rydosz, A.; Brzozowska, E.; Górska, S.; Wincza, K.; Gamian, A.; Gruszczynski, S. A Broadband Capacitive Sensing Method for Label-Free Bacterial LPS Detection. *Biosens. Bioelectron.* **2016**, *75*, 328–336. [CrossRef] [PubMed]

25. Bonincontro, A.; Risuleo, G. Dielectric Spectroscopy as a Probe for the Investigation of Conformational Properties of Proteins. *Spectrochim. Acta A Mol. Biomol. Spectrosc.* **2003**, *59*, 2677–2684. [CrossRef]
26. Narayanan, P.M. Microstrip Transmission Line Method for Broadband Permittivity Measurement of Dielectric Substrates. *IEEE Trans. Microw. Theory Tech.* **2014**, *62*, 2784–2790. [CrossRef]
27. Liu, S.; Ocket, I.; Barmuta, P.; Markovic, T.; Lewandowski, A.; Schreurs, D.; Nauwelaers, B. Broadband dielectric spectroscopy calibration using calibration liquids with unknown permittivity. In Proceedings of the 84th ARFTG Microwave Measurement Conference, Boulder, CO, USA, 4–5 December 2014.
28. Paredes, J.; Becerro, S.; Arizti, F.; Aguinaga, A.; Del Pozo, J.L.; Arana, S. Interdigitated Microelectrode Biosensor for Bacterial Biofilm Growth Monitoring by Impedance Spectroscopy Technique in 96-Well Microtiter Plates. *Sens. Actuat. B-Chem.* **2013**, *178*, 663–670. [CrossRef]
29. Bao, X.; Ocket, I.; Bao, J.; Doijen, J.; Zheng, J.; Kil, D.; Liu, Z.; Puers, B.; Schreurs, D.; Nauwelaers, B. Broadband dielectric spectroscopy of cell cultures. *IEEE Trans. Microw. Theory Tech.* **2018**, *12*, 5750–5759. [CrossRef]
30. Bao, J.; Maenhout, G.; Markovic, T.; Ocket, I.; Nauwelaers, B. A Microwave Platform for Reliable and Instant Interconnecting Combined with Microwave-Microfluidic Interdigital Capacitor Chips for Sensing Applications. *Sensors* **2020**, *20*, 1687. [CrossRef]
31. Grenier, K.; Dubuc, D.; Poleni, P.E.; Kumemura, M.; Toshiyoshi, H.; Fujii, T.; Fujita, H. Resonant Based Microwave Biosensor for Biological Cells Discrimination. In Proceedings of the 2010 IEEE Radio and Wireless Symposium (RWS), New Orleans, LA, USA, 10–14 January 2010.
32. Abduljabar, A.A.; Rowe, D.J.; Porch, A.; Barrow, D.A. Novel Microwave Microfluidic Sensor Using a Microstrip Split-Ring Resonator. *IEEE Trans. Microw. Theory Tech.* **2014**, *62*, 679–688. [CrossRef]
33. Jha, A.K.; Akhtar, M.J. A Generalized Rectangular Cavity Approach for Determination of Complex Permittivity of Materials. *IEEE Trans. Microw. Theory Tech.* **2014**, *63*, 2632–2641. [CrossRef]
34. Bao, J.; Yan, S.; Markovic, T.; Ocket, I.; Kil, D.; Brancato, L.; Puers, R.; Nauwelaers, B. A 20-GHz microwave miniaturized ring resonator for nL microfluidic sensing applications. *IEEE Sens. Lett.* **2019**, *6*, 1–4. [CrossRef]
35. Suster, M.A.; Mohseni, P. An RF/microwave microfluidic sensor based on a center-gapped microstrip line for miniaturized dielectric spectroscopy. In Proceedings of the 2013 IEEE MTT-S International Microwave Symposium Digest (MTT), Seattle, WA, USA, 2–7 June 2013; IEEE: Manhattan, NY, USA, 2013; pp. 1–3.
36. Veselago, V.G. Electrodynamics of Substances with Simultaneously Negative Values of ε and μ. *Sov. Phys. Uspekhi* **1967**, *10*, 509. [CrossRef]
37. RoyChoudhury, S.; Rawat, V.; Jalal, A.H.; Kale, S.N.; Bhansali, S. Recent Advances in Metamaterial Split-Ring-Resonator Circuits as Biosensors and Therapeutic Agents. *Biosens. Bioelectron.* **2016**, *86*, 595–608. [CrossRef] [PubMed]
38. Baena, J.D.; Bonache, J.; Martín, F.; Sillero, R.M.; Falcone, F.; Lopetegi, T.; Laso, M.A.; Garcia-Garcia, J.; Gil, I.; Portillo, M.F.; et al. Equivalent-Circuit Models for Split-Ring Resonators and Complementary Split-Ring Resonators Coupled to Planar Transmission Lines. *IEEE Trans. Microw. Theory Tech.* **2005**, *53*, 1451–1461. [CrossRef]
39. García-García, J.; Martin, F.; Falcone, F.; Bonache, J.; Gil, I.; Lopetegi, T.; Laso, M.A.; Sorolla, M.; Marqués, R. Spurious Passband Suppression in Microstrip Coupled Line Band Pass Filters by Means of Split Ring Resonators. *IEEE Microw. Wirel. Compon. Lett.* **2004**, *4*, 416–418. [CrossRef]
40. Ebrahimi, A.; Withayachumnankul, W.; Al-Sarawi, S.; Abbott, D. High-Sensitivity Metamaterial-Inspired Sensor for Microfluidic Dielectric Characterization. *IEEE Sens. J.* **2013**, *14*, 1345–1351. [CrossRef]
41. Puentes, M.; Maasch, M.; Schubler, M.; Jakoby, R. Frequency Multiplexed 2-Dimensional Sensor Array Based on Split-Ring Resonators for Organic Tissue Analysis. *IEEE Trans. Microw. Theory Tech.* **2012**, *60*, 1720–1727. [CrossRef]
42. Ansari, M.A.; Jha, A.K.; Akhter, Z.; Akhtar, M.J. Multi-Band RF Planar Sensor Using Complementary Split-Ring Resonator for Testing of Dielectric Materials. *IEEE Sens. J.* **2018**, *18*, 6596–6606. [CrossRef]
43. Ansari, M.A.; Jha, A.K.; Akhtar, M.J. Design and Application of the CSRR-Based Planar Sensor for Noninvasive Measurement of Complex Permittivity. *IEEE Sens. J.* **2015**, *15*, 7181–7189. [CrossRef]
44. Ansari, M.A.; Jha, A.K.; Akhtar, M.J. Dual Band Microwave Sensor for Dielectric Characterization of Dispersive Materials. In Proceedings of the 2015 Asia-Pacific Microwave Conference (APMC), Nanjing, China, 6–9 December 2015.
45. Lee, C.S.; Yang, C.L. Thickness and Permittivity Measurement in Multi-Layered Dielectric Structures Using Complementary Split-Ring Resonators. *IEEE Sens. J.* **2013**, *14*, 695–700. [CrossRef]
46. Maenhout, G.; Markovic, T.; Ocket, I.; Nauwelaers, B. Complementary Split-Ring Resonator with Improved Dielectric Spatial Resolution. *IEEE Sens. J.* **2020**, *21*, 4543–4552. [CrossRef]